Russ. J. Numer. Anal. Math. Modelling, Vol. 20, No. 4, pp. 391–402 (2005)

Hessian-based anisotropic mesh adaptation in domains with discrete boundaries

Yu. V. VASSILEVSKI,* V. G. DYADECHKO,† and K. N. LIPNIKOV†

Abstract — Black-box methodology for generating anisotropic adaptive tetrahedral meshes in domains with discrete boundaries is described. A new high-order reconstruction method for triangular surface meshes is proposed. The performance of the method for a model convection–diffusion problem is demonstrated.

To our Teacher

Adaptive methods greatly reduce the demand for a large number of unknowns and improve the accuracy of simulations via grid adaptation near fine-scale features of the solution. In this paper, we consider a tensor metric-based adaptive methodology [1, 3, 4, 6, 9, 15]. The metric is induced by an approximate Hessian (matrix of second derivatives) of the discrete solution. The focus of this paper is the treatment of curved internal and boundary surfaces.

In many applications the exact parameterization of curved surfaces may be unknown. In this case the surfaces are described by triangular meshes (e.g., meshes coming from CAD systems) which reduce the performance of adaptive methods due to a limited surface resolution. One possible solution is to use the results of adaptive computations as the feedback for CAD models. This approach usually requires the user's control and becomes too sophisticated for some applications. However, if the underlying surfaces are sufficiently smooth (or piecewise smooth), the original triangular meshes carry additional information regarding these surfaces. In this paper we use this fact to design a new surface reconstruction method and analyze it both theoretically and numerically.

There are many methods for higher-order reconstruction of piecewise linear surfaces (see 7, 10–12) and references therein). In [10, 12] the surface is parameterized and the desired surface characteristics are computed from the derivatives of functions specifying the parameterization. In [7, 10] the discrete surface is approximated by a piecewise quadratic surface using the best fit algorithm. The method proposed

*Institute of Numerical Mathematics, Russian Academy of Sciences, Moscow GSP-1, 119991, Russia; *E-mail*: vasilevs@dodo.inm.ras.ru

†Los Alamos National Laboratory, Theoretical Division, MS B284, Los Alamos, NM, 87545, USA; *E-mail*: {vdyadechko, lipnikov}@lanl.gov

The work was supported by the RFBR grant 04-07-90336 and academic program 'Computational and informatic issues of the solution of large problems'.

in this paper uses the technique of a discrete differential geometry to compute an approximate Hessian of a piecewise quadratic function representing the reconstructed surface. The Hessian is computed in a weak sense by analogy with the finite element methods. The developed method gives the exact solution for quadratic surfaces.

We demonstrate the efficiency of the new method for solving a convection-diffusion problem simulating transport phenomena around a spherical obstacle. The solution has a boundary layer along a part of the obstacle boundary. As the result, the accuracy of the discrete solution depends strongly on the accuracy of the boundary representation.

The paper outline is as follows. In Section 2 we describe briefly the Hessian-based adaptation methodology. In Section 3 we discuss two techniques for treatment of discrete surfaces. In Section 4 we illustrate our adaptive methodology with numerical tests.

1. HESSIAN-BASED MESH ADAPTATION

Let Ω_h be a mesh with $N(\Omega_h)$ elements and u_h be a discrete piecewise linear solution computed at the mesh nodes with some numerical method which we denote by $\mathscr{P}_{\Omega_h}$. We shall simply write that $u_h = \mathscr{P}_{\Omega_h} u$ where u is an unknown exact solution. The ideal goal would be to find a mesh (probably anisotropic) which minimizes the maximal norm of the discretization error $\|u - \mathscr{P}_{\Omega_h} u\|_\infty$. In many problems this error can be majorized by the interpolation error, $\|u - \mathscr{I}_{\Omega_h} u\|_\infty$, where $\mathscr{I}_{\Omega_h}$ is the linear interpolation operator on the mesh Ω_h. It gives us the following mesh optimization problem:

$$\Omega_h^{\text{opt}} = \arg \min_{N(\Omega_h) < N_{\max}} \|u - \mathscr{I}_{\Omega_h} u\|_\infty \tag{1.1}$$

where $N_{\max}$ is the maximal number of mesh elements (tetrahedra) defined by the user. This problem was analyzed both theoretically and numerically in [1, 15]. In fact, problem (1.1) was replaced by a simpler problem which provides a constructive way for finding an approximate solution of (1.1), or a quasi-optimal mesh. The latter is quasi-uniform in the metric $|H^h|$ derived from the discrete Hessian H^h of the discrete solution u_h. The generation of quasi-uniform meshes is based on the notion of the *mesh quality*.

Let G be a metric generated by a symmetric positive definite 3×3 matrix whose entries depend on the point $\mathbf{x} \in \Omega$. For an element e in Ω_h, we denote by $|e|_G$ its volume in metric G and by $|\partial\partial e|_G$ the total length of its edges (also in metric G). We define the mesh quality as

$$Q(\Omega_h) = \min_{e \in \Omega_h} Q(e) \tag{1.2}$$

where $Q(e)$ is the quality of a single element e,

$$Q(e) = 6\sqrt[4]{2} \frac{|e|_G}{|\partial\partial e|_G^3} F\left(\frac{|\partial\partial e|_G}{6h^*}\right), \qquad 0 < Q(e) \leqslant 1. \tag{1.3}$$

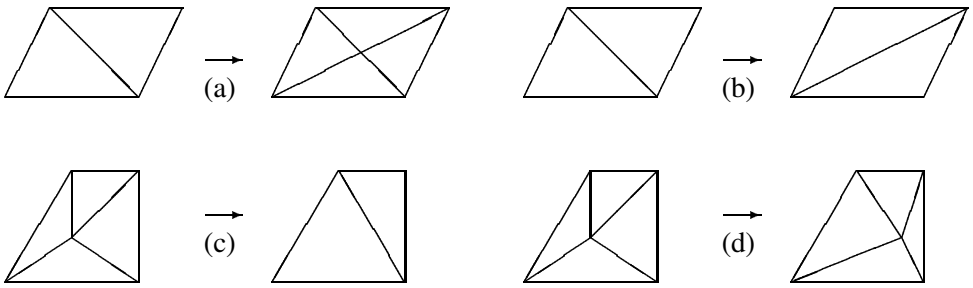

Figure 1. Local topological operations for 2D triangular meshes: (a) node insertion, (b) edge swapping, (c) node deletion, and (d) node movement.

Here h^* is the mesh size in the G-uniform mesh with $N_{\max}$ elements and $F(t)$ is a continuous smooth function, $0 \leqslant F(t) \leqslant 1$, with the only maximum at point 1, $F(1) = 1$, and such that $F(0) = F(+\infty) = 0$. The last factor in (1.3) controls the size of the element, whereas the remaining factors control its shape.

The optimization of the mesh Ω_h with respect to the mesh quality (1.2) results in the G-quasi-uniform grid. Since the mesh quality is as good as the quality of its worst element, the mesh improvement can be achieved with a series of *local* operations applied to this element. The list of such operations includes alternations of topology with node deletion/insertion, edge/face swapping, and node movement (see Fig. 1 for 2D analogs of local operations and [1] for more details).

Such local operations as node deletion/insertion and edge/face swapping are well described in the literature. The implementation of node movement requires additional comments. It is driven by the minimization of the smooth functional $\mathscr{F}$: $\mathbb{R}^3 \to \mathbb{R}$, of the node position $\mathbf{x}$, defined as a reciprocal of the mesh quality (1.2), i.e. $1 \leqslant \mathscr{F} < \infty$.

Some restrictions have to be imposed on mesh modifications to keep the mesh unfolded and to preserve internal and boundary surfaces. For example, the node movement should not alter the sign of the oriented volumes of the surrounding tetrahedra. Additionally, if a node lives on a surface, its movement should be restricted to this surface. In the next section we consider this problem in more detail.

Now we are ready to describe the iterative adaptive algorithm for the approximate solution of (1.1). Let us assume that an initial mesh is given. We begin with computing a discrete solution u_h and generating the Hessian-based metric $|H^h|$ which is the symmetric positive definite matrix given by

$$H^h = W_h \Lambda_h W_h^T, \qquad |H^h| = W_h |\Lambda_h| W_h^T$$

where W_h is the orthonormal matrix, $\Lambda_h = \operatorname{diag}\{\lambda_1, \lambda_2, \lambda_3\}$ is the diagonal matrix, and $|\Lambda_h| = \operatorname{diag}\{\max\{|\lambda_1|;\varepsilon\}, \max\{|\lambda_2|;\varepsilon\}, \max\{|\lambda_3|;\varepsilon\}\}$ with $\varepsilon > 0$ being a user-defined tolerance. Then, we use local operations to build a mesh which is quasi-uniform in metric $|H^h|$ and proceed with computing a new discrete solution and a new metric. If the mesh does not require any modifications, i.e. it is already quasi-

uniform, we terminate the adaptation procedure and refer to the resulting mesh as the *quasi-optimal* mesh.

It is proved in [1] that quasi-optimal meshes in polyhedral domains yields the asymptotically optimal estimate:

$$\|u - \mathscr{I}_{\Omega_h} u\|_\infty \sim N(\Omega_h)^{-2/3}. \tag{1.4}$$

In Section 4 we demonstrate numerically that (1.4) holds in a more general case of curved boundaries. We also show that the optimal estimate is violated when these boundaries are represented by triangular meshes.

2. TREATMENT OF INTERNAL AND BOUNDARY SURFACES

The distinctive geometrical features of any model are internal and boundary surfaces (*feature surfaces*) and their intersections (*feature edges*). Let us consider a particular feature surface $\Gamma \subset \mathbb{R}^3$ and a feature edge $\Theta \subset \mathbb{R}^3$. In many cases analytic information on these geometric features is not available and the only way to model them is to use faces and edges of the original mesh.

Let the discrete feature surface Γ_h be the triangulated surface of the original mesh Ω_h approximating Γ with triangular faces $\{\Gamma_t\}$, $\Gamma_h = \bigcup_t \Gamma_t$, and the discrete feature edge Θ_h be a polyline formed by the edges of Ω_h approximating Θ. We describe the discrete geometric features using parametric spaces $\mathscr{S}_\Theta$, $\mathscr{S}_\Gamma$ and maps $\mathscr{M}_\Theta$, $\mathscr{M}_\Gamma$ such that

$$\mathscr{M}_\Theta \colon \mathscr{S}_\Theta \to \Theta_h, \qquad \mathscr{M}_\Gamma \colon \mathscr{S}_\Gamma \to \Gamma_h.$$

In this section we consider two techniques for treatment of Γ_h and Θ_h. The first technique addresses the problem of a node movement along this piecewise linear surface. The second technique describes a new surface reconstruction method.

2.1. Node movement along a piecewise linear surface

In order to preserve geometrical features Θ_h and Γ_h during mesh modifications one has (a) to allow resident nodes to move only over the corresponding discrete features and (b) to forbid creation of new edges and faces which intersect these features. Hereafter, we focus on the most complicated constrained local operation, node movement.

While the global parameterization of the discrete feature edge Θ_h represented by a polyline is trivial, the definition of the global parametric space S_Γ for the discrete feature surface Γ_h is pretty tricky. The restriction $\mathscr{F}|_{\Gamma_h}$ of the objective function $\mathscr{F}$ to Γ_h is expected to have discontinuous normal derivatives on every sharp edge between constitutent faces. This complicates the global parameterization. However, the latter is not a priority: we introduce a separate parametric space for every face composing Γ_h [8] and use standard numerical tools of smooth optimization to move a node over a constituent face. Once the boundary of the local parametric space is

hit, the algorithm will use gradient information to make a decision whether to stay within a current parametric space or to switch to a new one.

We propose to use a *line search method* [2, 13] for node movement and the *barycentric* parameterization of constituent faces Γ_t for S_Γ. With barycentric parameterization, one can easily keep track of the boundaries of the triangular face: if $(\beta_1, \beta_2, \beta_3)$ and $(\Delta\beta_1, \Delta\beta_2, \Delta\beta_3)$ are barycentric coordinates of the node position and the search direction respectively, then the maximum step size allowed is

$$\min_{n=1,2,3} \{\max\{-\beta_n/\Delta\beta_n; 0\}\}.$$

The search over the triangulated surface can be identified as one of the three different states:

(1) moving over the face;
(2) moving along the edge;
(3) staying at the vertex.

Whenever the search is in State 1 and the face edge is reached, the steepest descent direction of $\mathscr{F}|_{\Gamma_h}$ (the restriction of $\mathscr{F}$ to Γ_h) may guide the further search either to stick with the current face, or to maintain State 1 switching to the adjacent face, or to continue along the edge (switch to State 2).

In State 2 the node motion is governed by the minimization of the function $\mathscr{F}|_\ell$ where ℓ denotes the mesh edge. If the local minimum is found at one of the ends of ℓ, the search comes to State 3. Otherwise the local minimum of $\mathscr{F}|_\ell$ can be located within the edge. Once this minimum is reached, one has to evaluate one-sided ℓ-normal derivatives of $\mathscr{F}|_{\Gamma_h}$, one per each adjacent edge. If the objective function decreases as we approach the edge from either side, then the search is over: we have found a local minimum of the $\mathscr{F}|_{\Gamma_h}$. If not, the search should be continued over the adjacent face which guarantees the steepest descent.

The strategy in State 3 is pretty straightforward: find the face (or edge) that provides the steepest descent and switch to State 1 (or State 2, respectively). If there is no descent direction found, the search is over: we are at the local minimum.

2.2. Piecewise quadratic extrapolation of piecewise linear surfaces

In this section we consider again the feature surface Γ. To simplify the presentation, we assume that Θ is its boundary. We assume also that the nodes of Γ_h and Θ_h belong to Γ and Θ, respectively, although this assumption is not necessary in practice. The piecewise quadratic extrapolation $\tilde{\Gamma}_h$ of Γ_h is defined as the continuous surface being the closure of a union of open non-overlapping pieces $\tilde{\Gamma}_t$ of local quadratic extrapolations over faces Γ_t.

The local extrapolation $\tilde{\Gamma}_t$ is described by a quadratic function $\varphi_{2,t}$. We shall omit the superscript t whenever it does not result in confusion. For our purposes, it will be convenient to describe the function φ_2 in a local coordinate system (ξ_1, ξ_2)

associated with the plane of Γ_t. In this coordinate system, the 2D multi-point Taylor formula for a quadratic function φ_2 with the Hessian $H^{\varphi_2} = \{H^{\varphi_2}_{ps}\}_{p,s=1}^{2}$ reads

$$\varphi_2(\boldsymbol{\xi}) = -\frac{1}{2}\sum_{i=1}^{3}(H^{\varphi_2}(\boldsymbol{\xi} - \mathbf{a}_i), (\boldsymbol{\xi} - \mathbf{a}_i))\, p_i(\boldsymbol{\xi}) \tag{2.1}$$

where $\mathbf{a}_1$, $\mathbf{a}_2$, $\mathbf{a}_3$ are the vertices of the triangle Γ_t and $p_i(\boldsymbol{\xi})$ is a piecewise linear function such that $p_i(\mathbf{a}_j) = \delta_{ij}$.

In order to recover the Hessian H^{φ_2}, we *first* assume that numbers $\alpha_i = (H^{\varphi_2}\ell_i, \ell_i)$, $i = 1, 2, 3$, representing the projection of this Hessian on edges ℓ_i of Γ_t are given. Hereafter, we use ℓ_i for both the mesh edge and the corresponding vector. In the local coordinate system, vectors ℓ_i are described by two coordinates, $\ell_i = (l_1^i, l_2^i)$. We assume that vector ℓ_i begins at the vertex $\mathbf{a}_i$ and ends at the vertex $\mathbf{a}_{i+1}$ with $\mathbf{a}_4 = \mathbf{a}_1$. Then, the definition of α_i gives

$$\left(\begin{pmatrix} H_{11}^{\varphi_2} & H_{12}^{\varphi_2} \\ H_{12}^{\varphi_2} & H_{22}^{\varphi_2} \end{pmatrix}\begin{pmatrix} l_1^i \\ l_2^i \end{pmatrix}, \begin{pmatrix} l_1^i \\ l_2^i \end{pmatrix}\right) = \alpha_i$$

which, in turn, results in the system of three linear equations for the unknown entries of the matrix H^{φ_2}:

$$l_1^i l_1^i H_{11}^{\varphi_2} + l_2^i l_2^i H_{22}^{\varphi_2} + 2\, l_1^i l_2^i H_{12}^{\varphi_2} = \alpha_i, \qquad i = 1, 2, 3. \tag{2.2}$$

Lemma 2.1. *The matrix of system* (2.2) *is non-singular.*

Proof. Let us denote the coefficient matrix of system (2.2) by B. Note that $\ell_1 + \ell_2 + \ell_3 = 0$. Using this fact in direct calculations of the determinant of matrix B we get

$$|\det B| = 2|l_1^1 l_2^2 - l_1^2 l_2^1|^3 = 16|\Gamma_t|^3 > 0 \tag{2.3}$$

where $|\Gamma_t|$ is the area of the triangle Γ_t. This proves the assertion of the lemma.

Second, we use the results of [1] where the algorithm for computing discrete Hessian $H^h(\mathbf{a}_i)$ at a vertex $\mathbf{a}_i$ of a continuous piecewise linear solution is presented and analyzed. We define α_i as the average of two nodal approximations,

$$\alpha_i = \frac{1}{2}((H^h(\mathbf{a}_i)\ell_i, \ell_i) + (H^h(\mathbf{a}_{i+1})\ell_i, \ell_i)) \tag{2.4}$$

associated with the edge ℓ_i. There are two exceptions from this rule. If $\mathbf{a}_i \in \Theta_h$ and $\mathbf{a}_{i+1} \notin \Theta_h$, then α_i is equal to $(H^h(\mathbf{a}_{i+1})\ell_i, \ell_i)$. If $\mathbf{a}_i \in \Theta_h$ and $\mathbf{a}_{i+1} \in \Theta_h$, then $\alpha_i = 0$. This implies that the nodal approximation of the Hessian is not recovered at feature edges and, therefore, the traces of Γ_h and $\tilde{\Gamma}_h$ on Θ_h coincide.

It remains to describe how we recover $H^h(\mathbf{a}_i)$ for every interior node $\mathbf{a}_i$ of Γ_h. We begin by introducing a few additional notations. For each $\mathbf{a}_i$, we define the superelement σ_i as a union of all triangles of Γ_h sharing $\mathbf{a}_i$. Then, we define a plane

approximating in the least square sense the nodes of this superelement and associate this plane with the local coordinate system (ξ_1, ξ_2)-plane. Let $\hat{\sigma}_i$ be the projection of σ_i onto the (ξ_1, ξ_2)-plane. Further, let $\varphi^i(\xi_1, \xi_2)$ be the continuous function representing locally Γ and $\varphi_h^i(\xi_1, \xi_2)$ be the continuous piecewise linear function representing σ_i. We assume that both functions are single-valued over $\hat{\sigma}_i$. Finally, we denote the Hessian of φ by H^φ.

The components of the discrete Hessian H^h are defined in a weak sense by

$$\int_{\hat{\sigma}_i} H^h_{ps}(\mathbf{a}_i)\,\psi_h \,\mathrm{d}S = -\int_{\hat{\sigma}_i} \frac{\partial \varphi_h^i}{\partial \xi_p}\frac{\partial \psi_h}{\partial \xi_s}\,\mathrm{d}S, \qquad p,s = 1,2 \tag{2.5}$$

which holds for any continuous piecewise linear function ψ_h vanishing on $\partial\hat{\sigma}_i$. Note that the discrete Hessian $H^h(\mathbf{a}_i)$ is a geometric characteristic of the feature surface Γ at the point $\mathbf{a}_i$ (related to its curvature) and, therefore, is invariant of the position of the projection plane associated with the superelement σ_i. In other words, the value $(H^h(\mathbf{a}_i)\ell_i, \ell_i)$ is independent of the local transformation of the coordinate system.

In addition to the above invariance and the obvious uniqueness of H^h, the specified extrapolation is exact for quadratic surfaces, as long as the triangle Γ_t has no edges on Θ_h. Indeed, for a quadratic function φ the recovery method (2.5) is exact, i.e. $H^h_{ps}(\mathbf{a}_i) = H^\varphi_{ps}(\mathbf{a}_i)$. Therefore, for all $\mathbf{a}_i \notin \Theta_h$

$$(H^\varphi \ell, \ell) = (H^h(\mathbf{a}_i)\ell, \ell)$$

for all edges $\ell \subset \Gamma_h \setminus \Theta_h$ and $H^{\varphi_2} = H^\varphi$ follows from (2.4) and Lemma 2.1.

Now we consider the approximation property of our extrapolation method. For every triangle Γ_t we define a superelement σ^t as a union of superelements σ_i corresponding to vertices $\mathbf{a}_i$ of Γ_t. Again, we use the local coordinate system (ξ_1, ξ_2)-plane associated with the triangle Γ_t. Let $\hat{\sigma}^t$ (respectively, $\hat{\Gamma}_t$) be the projection of σ^t (respectively, Γ_t) onto the (ξ_1, ξ_2)-plane. We define the constant tensor $H^\varphi_{\sigma^t}$ for the superelement $\hat{\sigma}^t$ as

$$H^\varphi_{\sigma^t} = H^\varphi\Big(\arg \max_{\xi \in \hat{\sigma}^t} |\det H^\varphi(\xi)|\Big). \tag{2.6}$$

Proposition 2.1. *Let the edges of a triangle Γ_t be the interior edges of Γ_h and $\hat{\sigma}_t$ be a quasi-uniform triangulation with a size h. Let $\varphi(\xi_1, \xi_2)$ be $C^2(\hat{\sigma}^t)$ function representing locally Γ and $\varphi_h = \mathscr{I}_{\hat{\sigma}^t}\varphi$ be a continuous piecewise linear function representing σ^t. Moreover, let H^φ and H^h be the differential and discrete Hessians of φ and φ_h, respectively, such that*

$$\|H^\varphi_{ps} - H^\varphi_{\sigma^t,ps}\|_{L_\infty(\hat{\sigma}^t)} < \delta \tag{2.7}$$

$$\|\nabla(\varphi - \mathscr{I}_{\hat{\sigma}^t}\varphi)\|_{L_2(\hat{\sigma}^t)} < \varepsilon. \tag{2.8}$$

Then, the quadratic function φ_2 describing $\tilde{\Gamma}_t$ by (2.1), (2.2), (2.4) *and* (2.5) *satisfies*

$$\|\varphi - \varphi_2\|_{L_\infty(\hat{\Gamma}_t)} \leqslant C(\varepsilon + \delta h^2) \tag{2.9}$$

where a constant C is independent of δ, ε, h and φ.

Proof. Hereinafter we shall use notations C, C_i for generic constants having different values in different places. The definition (2.5) of the discrete Hessian implies that

$$\int_{\hat{\sigma}_i} (H^{\varphi}_{ps} - H^h_{ps}(\mathbf{a}_i))\,\psi_h \,\mathrm{d}S = -\int_{\hat{\sigma}_i} \frac{\partial(\varphi-\varphi_h)}{\partial\xi_p}\frac{\partial\psi_h}{\partial\xi_s}\,\mathrm{d}S \tag{2.10}$$

for any $\psi_h \in P_1(\hat{\sigma}_i)$ vanishing on $\partial\hat{\sigma}_i$. Now, using the triangle inequality and then the Cauchy inequality, we get

$$\begin{aligned}\int_{\hat{\sigma}_i} |H^{\varphi}_{\sigma^t,ps} - H^h_{ps}(\mathbf{a}_i)|\,|\psi_h|\,\mathrm{d}S \;\leqslant\; & \left\|\frac{\partial(\varphi-\varphi_h)}{\partial\xi_p}\right\|_{L_2(\hat{\sigma}_i)} \left\|\frac{\partial\psi_h}{\partial\xi_s}\right\|_{L_2(\hat{\sigma}_i)} \\ & + \int_{\hat{\sigma}_i} |H^{\varphi}_{\sigma^t,ps} - H^{\varphi}_{ps}|\,|\psi_h|\,\mathrm{d}S.\end{aligned}$$

Let us evaluate all terms in the above inequality for a particular choice of ψ_h such that $\psi_h(\mathbf{a}_i) = 1$. The term in the left-hand side is estimated from below as follows:

$$\int_{\hat{\sigma}_i} |H^{\varphi}_{\sigma^t,ps} - H^h_{ps}(\mathbf{a}_i)|\,\psi_h\,\mathrm{d}S \geqslant C_1 |H^{\varphi}_{\sigma^t,ps} - H^h_{ps}(\mathbf{a}_i)|\,|\hat{\sigma}_i|.$$

The terms in the right-hand side may be easily estimated from above using the quasi-uniformity of $\hat{\sigma}^t$ and assumption (2.7):

$$\left\|\frac{\partial\psi_h}{\partial\xi_s}\right\|_{L_2(\hat{\sigma}_i)} \leqslant C_2, \qquad \int_{\hat{\sigma}_i} |H^{\varphi}_{\sigma^t,ps} - H^{\varphi}_{ps}|\,\psi_h\,\mathrm{d}S \leqslant C_3\delta|\hat{\sigma}_i|.$$

Combining the above inequalities, we get

$$|H^{\varphi}_{\sigma^t,ps} - H^h_{ps}(\mathbf{a}_i)| \leqslant \frac{C_2}{C_1|\hat{\sigma}_i|}\varepsilon + \frac{C_3}{C_1}\delta. \tag{2.11}$$

Let H^{φ_2} be the Hessian of the quadratic function φ_2. The next step in the proof is to estimate the discrepancy between $H^{\varphi}_{\sigma^t}$ and H^{φ_2}. For this purpose, we use the perturbation analysis and Lemma 2.1. Since both Hessians $H^{\varphi}_{\sigma^t}$, H^{φ_2} are constant, they are uniquely defined by the right-hand side of system (2.2) and the edges of the triangle Γ_t. Let α_1, α_2 and α_3 be the entries of the right-hand side in (2.2) whose solution is $H^{\varphi_2}_{ps}$, and let $\beta_i = (H^{\varphi}_{\sigma^t}\ell_i, \ell_i)$, $i = 1,2,3$. Using definition (2.4), inequality (2.11), a linear algebra estimate for eigenvalues of a 2×2 matrix, and the assumption of quasi-uniformity of $\hat{\sigma}^t$, we get

$$\begin{aligned}|\alpha_i - \beta_i| \;&=\; \frac{1}{2}|(H^h(\mathbf{a}_i)\ell_i, \ell_i) + (H^h(\mathbf{a}_{i+1})\ell_i, \ell_i) - 2(H^{\varphi}_{\sigma^t}\ell_i, \ell_i)| \\ &\leqslant\; 2\left(\frac{C_2\varepsilon}{C_1 \min\limits_{i=1,2,3}|\hat{\sigma}_i|} + \frac{C_3}{C_1}\delta\right)(\ell_i, \ell_i) \leqslant C(\varepsilon + \delta h^2).\end{aligned}$$

The perturbation analysis states that

$$|H^{\varphi_2}_{ps} - H^{\varphi}_{\sigma^t,ps}| \leqslant C\,|\lambda^{-1}_{\min}(B)| \max_{i=1,2,3} |\alpha_i - \beta_i|$$

where the matrix B is defined in Lemma 2.1 and $\lambda_{\min}(B)$ is its eigenvalue closest to zero. The application of the Gershgorin theorem and the quasi-uniformity assumption give the estimate for the maximal eigenvalue of B:

$$\lambda_{\max}(B) \leqslant 2 \max_{1\leqslant i\leqslant 3} |\ell_i|^2 \leqslant Ch^2.$$

Therefore, due to (2.3)

$$|\lambda_{\min}(B)| \geqslant \frac{|\det B|}{\lambda^2_{\max}(B)} = \frac{16|\Gamma_t|^3}{\lambda^2_{\max}(B)} \geqslant Ch^2.$$

Using the last estimate, we get easily

$$|H^{\varphi}_{\sigma^t,\,ps} - H^{\varphi_2}_{ps}| \leqslant C(\varepsilon/h^2 + \delta). \tag{2.12}$$

Finally, by virtue of the multi-point Taylor formula for a general function φ whose linear interpolant φ_h vanishes on the triangle $\hat{\Gamma}_t = \Gamma_t$ we get:

$$\varphi(\boldsymbol{\xi}) = -\frac{1}{2}\sum_{i=1}^{3}(H^{\varphi}(\boldsymbol{\xi}^*_i)(\boldsymbol{\xi} - \mathbf{a}_i),\,(\boldsymbol{\xi} - \mathbf{a}_i))\,p_i(\boldsymbol{\xi})$$

where $\boldsymbol{\xi}^*_i(\boldsymbol{\xi})$ is a point inside $\hat{\Gamma}_t$, $\boldsymbol{\xi} \in \Gamma_t$. Together with formula (2.1) it gives

$$|\varphi(\boldsymbol{\xi}) - \varphi_2(\boldsymbol{\xi})| = \frac{1}{2}\left|\sum_{i=1}^{3}([H^{\varphi}(\boldsymbol{\xi}^*_i) - H^{\varphi_2}](\boldsymbol{\xi} - \mathbf{a}_i),\,(\boldsymbol{\xi} - \mathbf{a}_i))\,p_i(\boldsymbol{\xi})\right| \leqslant C(\varepsilon + \delta h^2).$$

This proves the assertion of the proposition.

Generally speaking, the values of ε and δ depend on the derivatives of φ. If φ is sufficiently smooth, for example it is in $C^3(\hat{\sigma}^t)$, then $\varepsilon \sim h^3$ [5], $\delta \sim h$ and we get the expected result

$$\|\varphi - \varphi_2\|_{L_\infty(\hat{\Gamma}_t)} \leqslant Ch^3.$$

3. NUMERICAL EXPERIMENTS

We consider the following convection-diffusion equation as the model problem:

$$\begin{aligned} -0.01\Delta u + \mathbf{b}\cdot\nabla u &= 0 \quad \text{in } \Omega \\ u &= g \quad \text{on } \Gamma_{\text{in}} \\ \frac{\partial u}{\partial n} &= 0 \quad \text{on } \Gamma_{\text{out}} \\ u &= 0 \quad \text{on } \partial\Omega \setminus (\Gamma_{\text{in}} \cup \Gamma_{\text{out}}). \end{aligned} \tag{3.1}$$

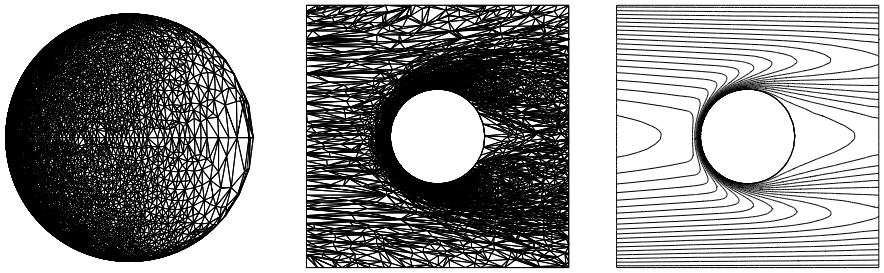

(a) (b) (c)

Figure 2. (a) Mesh trace at the obstacle, (b) mesh cut and (c) isolines of solution u_* on the plane passing through the center of the obstacle and parallel to the x_1x_2-plane.

Here $\mathbf{b} = (1,0,0)^T$ is the velocity field, $\Omega = (0,1)^3 \setminus B_{0.5}(0.18)$ is the computational domain with $B_{0.5}(r) = \{\mathbf{x}\colon\ \sum_{i=1}^3 (x_i - 0.5)^2 \leqslant r^2\}$, $\Gamma_{\text{in}} = \{\mathbf{x} \in \partial\Omega\colon\ x_1 = 0\}$, $\Gamma_{\text{out}} = \{\mathbf{x} \in \partial\Omega\colon\ x_1 = 1\}$, and $g(x_2,x_3) = 16x_2(1-x_2)x_3(1-x_3)$ is the standard Poiseile profile of the incoming flow.

The solution u to (3.1) possesses a boundary layer along the upwind side of the spherical obstacle $B_{0.5}(0.18)$ and is very smooth in the shadow region of this obstacle. Since the exact solution is not known, in our experiments we replace it with the piecewise linear finite element solution u_* computed on a very fine adaptive (quasi-optimal) mesh containing more than 1.28 million tetrahedra (see Fig. 2). To build the adaptive mesh, we used the analytical representation of $\partial\Omega$.

In the first set of experiments (Fig. 3a) we demonstrate the asymptotic result (1.4) with u_* instead of u. The L_∞ error fits the analytic curve $60N(\Omega_h)^{-2/3}$.

In the second set of experiments (Fig. 3b), the boundary $\Gamma = \partial B_{0.5}(0.18)$ is approximated with a quasi-uniform mesh Γ_h. We determine the L_∞ error as a function of $N(\Omega_h)$ for three different values of h. Figure 3 shows the saturation of this error due to the limited boundary resolution. We observe that the saturated error θ_h is almost reciprocal to h^2: $\theta_{0.05} = 0.20$, $\theta_{0.025} = 0.067$, and $\theta_{0.0125} = 0.021$. This is probably related to the second-order approximation of the smooth boundary Γ by the piecewise linear manifold Γ_h.

In the third set of experiments (Fig. 3c), we study the effect of the piecewise quadratic extrapolation $\tilde{\Gamma}_h$ of Γ_h on the accuracy of the discrete solution. We compare the saturation errors for three meshes: $\Gamma_{0.025}$, $\Gamma_{0.0125}$ and $\Gamma^*_{0.0125}$. The third mesh is obtained from $\Gamma_{0.0125}$ by projecting its mesh nodes onto $\tilde{\Gamma}_{0.025}$. This mesh must provide the saturation error θ^*_h which is between the saturation errors on the other two meshes. This is illustrated in Fig. 3 where $\theta_{0.0125} = 0.021$, $\theta_{0.025} = 0.067$, and $\theta^*_{0.0125} = 0.043$.

Another approach for building a piecewise linear surface $\Gamma^*_{0.0125}$ is based on the uniform refinement of $\Gamma_{0.025}$ with a subsequent projection of new mesh nodes onto $\tilde{\Gamma}_{0.025}$. We use the first approach because it gives the most rigorous comparison of saturation errors on meshes $\Gamma_{0.0125}$ and $\Gamma^*_{0.0125}$.

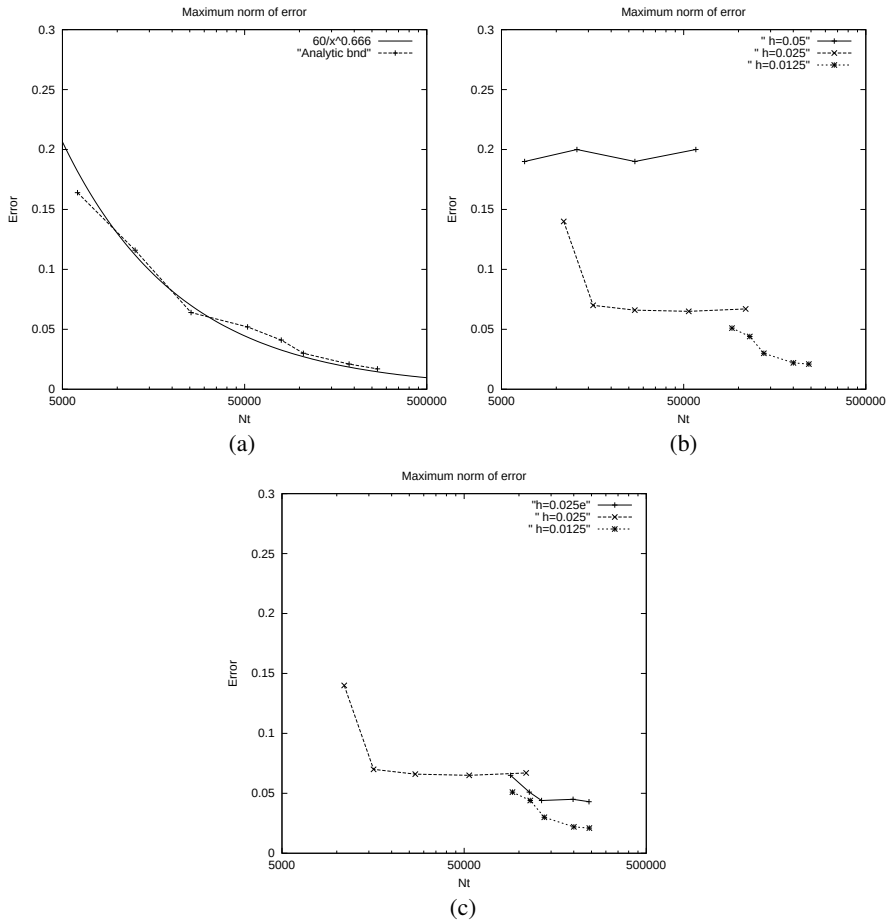

Figure 3. Convergence analysis: (a) using analytic representation of the obstacle boundary, (b) using three discrete models $\Gamma_{0.05}$, $\Gamma_{0.025}$, and $\Gamma_{0.0125}$ for $\partial B_{0.5}(0.18)$, (c) using piecewise quadratic extrapolation $\tilde{\Gamma}_{0.025}$.

In practice, the surface reconstruction should be dynamic and driven by the size of mesh elements. For convection-diffusion problem (3.1) the surface extrapolation is required only in the upwind part of the obstacle boundary. We shall address this problem in the future.

4. CONCLUSION

We have shown that representation of curved surfaces using triangular meshes restricts the use of adaptive methods. From the implementation viewpoint, an efficient technique for node movement over discrete surfaces has to be elaborated. We have presented an example of such a technique. From the theoretical viewpoint, the use of triangular meshes instead of analytic surfaces complicates the analysis of adaptive

methods. For a particular convection-diffusion problem, we have shown numerically that the discretization error is proportional to h^2 where h is the size of the quasi-uniform mesh approximating the curved surface. We have analyzed theoretically and numerically a new surface reconstruction technique, which improves the performance of adaptive methods.

Acknowledgement

The authors are very grateful to N. L. Zamarashkin for valuable comments.

REFERENCES

1. A. Agouzal, K. Lipnikov, and Yu. Vassilevski, Adaptive generation of quasi-optimal tetrahedral meshes. *East-West J. Numer. Math.* (1999) **7**, No. 4, 223–244.
2. J. F. Bonnans, C. Gilbert, C. Lemarécha, and C. A. Sagastizábal, *Numerical Optimization. Theoretical and Practical Aspects*. Springer-Verlag, Berlin, 2003.
3. H. Borouchaki, F. Hecht, and P. J. Frey, Mesh gradation control. *Inter. J. Numer. Meth. Engrg.* (1998) **43**, 1143–1165.
4. G. C. Buscaglia and E. A. Dari, Anisotropic mesh optimization and its application in adaptivity. *Inter. J. Numer. Meth. Engrg.* (1997) **40**, 4119–4136.
5. P. G. Ciarlet, *The Finite Element Method for Elliptic Problems*. North-Holland, Amsterdam, 1978.
6. J. Dompierre, M.-G. Vallet, M. Fortin, W. G. Habashi, D. Ait-Ali-Yahia, and A. Tam, Edge-based mesh adaptation for CFD. *CERCA Report No. 95–73*, 1995.
7. R. V. Garimella and B. K. Swartz, Curvature estimation for unstructured triangulations of surfaces. *Los Alamos Report No. LA-UR-03-8240*, Los Alamos, NM, http://math.lanl.gov/Research/Publications/Docs/garimella-2003-curvature.pdf.
8. R. Garimella, P. Knupp, and M. Shashkov, Triangular and quadrilateral surface mesh quality optimization using local parameterization. *Comp. Meth. Appl. Mech. Engrg.* (2004) **193**, No. 9–11, 913–928.
9. K. Lipnikov and Yu. Vassilevski, Parallel adaptive solution of 3D boundary value problems by Hessian recovery. *Comp. Meth. Appl. Mech. Engrg.* (2003) **192**, 1495–1513.
10. A. M. McIvor and R. J. Valkenburg, A comparison of local surface geometry estimation methods. *Machine Vision and Appl.* (1997) **10**, 17–26.
11. M. Meyer, H. Lee, A. H. Barr, and M. Desbrun, Generalized barycentric coordinates on irregular polygons. *J. Graphics Tools* (2002) **7**, No. 1, 13–22.
12. F. Mokhtarian, N. Khalili, and P. Yuen, Curvature computation of free-form 3-D meshes at multiple scales. *Comp. Vision and Image Understanding* (2001) **83**, 118–139.
13. J. Nocedal and S. J. Wright, *Numerical Optimization*. Springer-Verlag, New York, 1999.
14. S. Petitjean, A survey of methods for recovering quadrics in triangle meshes. *ACM Comp. Surveys* (2002) **32**, 211–262.
15. Yu. Vassilevski and K. Lipnikov, Optimal triangulations: existence, approximation and double differentiation of P_1 finite element functions. *Comp. Math. Math. Phys.* (2003) **43**, 827–835.